Induction of de novo α-Synuclein fibrillization in a novel neuronal model for Parkinson's disease

Mohamed-Bilal Fares[a], Bohumil Maco[a], Abid Oueslati[a], Edward Rockenstein[b], Natalia Ninkina[c], Vladimir Buchman[c], Eliezer Masliah[b], & Hilal A. Lashuel[a].

[a]Brain Mind Institute, Swiss Federal Institute of Technology Lausanne (EPFL), Lausanne, CH-1015, Switzerland; [b]Department of Neurosciences, University of California San Diego (UCSD), La Jolla, CA 92093-0624, USA; [c]School of Biosciences, Cardiff University, Cardiff, CF10 3AX,UK.

To whom correspondence should be addressed: Hilal A. Lashuel, Brain Mind Institute, Swiss Federal Institute of Technology Lausanne (EPFL), Lausanne, CH-1015, Switzerland. Phone: +41 21 69 39691; Email: hilal.lashuel@epfl.ch.

Conflict of Interest: The authors have declared that no conflict of interest exists.

Abstract (max 250 words)

Lewy bodies (LBs) are intra-neuronal inclusions consisting primarily of fibrillized human-α-Synuclein (hα-Syn) protein and represent the major pathological hallmark of Parkinson's disease (PD). Although doubling hα-Syn expression provokes LB pathology in humans, hα-Syn over-expression doesn't trigger authentic LB formation in mice. We hypothesized that this could be attributed to interactions between exogenous hα-Syn and its endogenous mouse α-Syn (mα-Syn) homologue, and investigated whether hα-Syn over-expression on mα-Syn KO backgrounds could promote hα-Syn fibrillization. Herein, we show that hα-Syn forms hyper-phosphorylated (at S129) and ubiquitin positive LB-like inclusions in mα-Syn KO primary neurons, as well as in transgenic mα-Syn KO mouse brains *in vivo*. Correlative light and electron microscopy, immuno-gold labelling and Thioflavin-S binding established their fibrillar ultrastructure, and FRAP/photo-conversion experiments showed that these inclusions grow in size and incorporate soluble proteins. Notably, hα-Syn inclusions were also observed upon knock-down of another mα-Syn homologue "β-Syn", thereby proposing a role for these homologous proteins as natural inhibitors of abnormal aggregation. Mechanistically, our data show that mα-Syn preferentially interacts with aggregated hα-Syn PFFs species, and that such a "cross-species" interaction does not promote progressive aggregation *in vitro* and *in vivo*. As such, endogenous mα-Syn could be attenuating hα-Syn aggregation in mice *via* direct interaction and capping of early fibrillar forms. Altogether, our results provide novel primary neuronal and *in vivo* models for understanding mechanisms underlying hα-Syn intra-neuronal fibrillization, the contribution of this process to PD pathogenesis, and for screening pharmacologic and genetic modulators of α-Syn fibrillization in neurons.

Keywords: Parkinson's disease, alpha-synuclein, aggregation.

Significance Statement (max 120 words)

Although it has been established for over 100 years that Lewy bodies (LBs) represent the major pathological hallmark of Parkinson's disease (PD), we still do not know why these fibrillar intra-neuronal inclusions of the α-Synuclein (α-Syn) protein form, and how they contribute to disease progression. One of the major causes underlying this gap in knowledge is the unavailability of animal models that truly reproduce the formation of LBs. In this study, we show that the lack of hα-Syn fibrillization into LBs in mouse models can be attributed to interactions between hα-Syn and its endogenously expressed mouse α-Syn homologue. Moreover, we provide novel well-characterized primary neuronal and *in vivo* models which recapitulate the main molecular feature of PD; bonafide α-Syn fibrillization.

\body

Introduction

The aggregation of proteins into fibrillar structures is a key hallmark of many neurodegenerative disorders. In Parkinson's disease (PD), α-synuclein (α-Syn), a predominantly pre-synaptic protein involved in regulation of neurotransmitter release, abnormally fibrilizes and forms intra-neuronal inclusions termed Lewy bodies (LBs)(1, 2). So far, the mechanisms underlying LB formation remain poorly understood, and the impact of LB presence on neuronal viability remains controversial, in part due to the lack of animal models recapitulating α-Syn fibrillization into authentic LBs.

Since patients with familial history of parkinsonism were found carrying either multiplications or point mutations of the α-Syn gene "*SNCA"(2)*, most animal models of PD have been generated by over-expressing wild-type (WT) human α-Syn (hα-Syn) or mutant forms linked with familial PD(3). Strikingly, whereas rodent models expressing hα-Syn do not recapitulate the formation of authentic LBs comprising fibrillar α-Syn within dopaminergic neurons, hα-Syn over-expression in *Drosophila* led to dramatic neuronal loss accompanied with fibrillar LB-like structures(4). The fact that *Drosophila*, unlike rodents, lack expression of an endogenous α-Syn homologue implied that hα-Syn fibril formation could be more favorable in models lacking endogenous α-Syn expression. Subsequent experiments in mice supported this suggestion, as hα-Syn transgenic (Tg) mice lacking endogenous mα-Syn exhibited exacerbated pathology compared to WT counterparts(5), and manifested fibrillar/granular accumulations in the olfactory bulb(6). Explaining this effect, *in vitro* "test-tube" experiments remarkably showed that small amounts of mouse α-Syn (mα-Syn) directly inhibit the fibrillization of purified hα-Syn protein in solution(7).

Despite all of these interesting observations, it remained unclear whether endogenously expressed Synuclein homologues directly inhibit hα-Syn aggregation in neurons, and whether ectopic hα-Syn expression in their absence would allow *de novo* hα-Syn fibrillization events. Therefore, we systematically evaluated the propensity of hα-Syn to aggregate on Synuclein KO backgrounds. Using a battery of biochemical and imaging techniques, we demonstrate that in cultured primary neurons and brains of mα-Syn KO mice, over-expressed hα-Syn readily aggregates into inclusions that exhibit several similarities with LBs in terms of solubility, immuno-reactivity and amyloidogenicity, and represent a bonafide fibrillization process as revealed by serial-section transmission electron microscopy (ssTEM), live imaging, and response to pharmacological aggregation inhibitors. Similarly, primary neurons lacking expression of β-Syn (β-Syn$^{-/-}$) or all three homologues (α- β- and γ- Syn) also manifest enhanced hα-Syn aggregation, thereby suggesting that the presence of endogenous Synuclein homologues may represent a natural mechanism regulating abnormal α-Syn aggregation. To dissect this mechanism, we performed immuno-precipitation and surface plasmon resonance experiments which intriguingly showed that mα-Syn preferentially interacts with aggregated hα-Syn PFFs species rather than monomers. Importantly, *in vitro* aggregation experiments and *in vivo* assessment of cross-seeding propensities showed that the observed

"cross-species" interactions do not promote progressive seeding and spreading of aggregates. These findings provide a possible explanation as to why current rodent PD models expressing hα-Syn do not exhibit pronounced hα-Syn fibrillization, and provide models that reproduce a critical pathological feature of the disease: the *de novo* formation of fibrillar hα-Syn aggregates.

Results

Induction of hα-Syn inclusion formation in *SNCA*$^{-/-}$ primary neurons

Several studies have previously reported that over-expressed hα-Syn in mouse primary neurons exhibits diffuse localization without forming discreet inclusions (8-11). To assess whether the absence of mα-Syn would affect this distribution, we examined the localization of transiently expressed hα-Syn in primary neurons derived from C57Bl6/J/ola/hsd mice (*SNCA*$^{-/-}$) lacking expression of mα-Syn(12) (Fig. S1A-B). Interestingly, whereas hα-Syn exhibited the previously reported diffuse distribution in WT neurons, a significant proportion of the *SNCA*$^{-/-}$ neurons developed spheroid-like inclusions that were consistently observed in close association with nuclear and cytoplasmic membranes (Fig. 1A and Video S1). A similar phenotype was observed in primary neurons derived from another *SNCA*$^{-/-}$ mouse strain (B6,129X1-*Snca*^{tm1Rosl}/J) generated by targeted deletion of two exons of the mα-Syn gene(13) (Fig. S2C-D), thereby establishing that inclusion formation is directly linked to the specific loss of mα-Syn expression. In line with this, re-expression of mα-Syn in *SNCA*$^{-/-}$ neurons significantly reduced the formation of intra-neuronal hα-Syn inclusions, and restored the diffuse distribution of hα-Syn in most neurons (Fig. 1B).

To investigate whether the total abolishment of mα-Syn expression is necessary to promote hα-Syn inclusion formation, we assessed whether decreasing mα-Syn levels in WT neurons *via* shRNA mediated silencing is sufficient to promote this process. Transient expression of three different vectors encoding shRNA hairpin loops (Fig. S2A) showed efficient silencing of mα-Syn in transfected neurons compared to those transfected with scrambled shRNA sequences (Fig. S2B), and biochemical analysis of lentivirally infected neurons showed over 50% reduction in mα-Syn expression (Fig. S2C). Notably however, silencing mα-Syn did not promote hα-Syn inclusion formation in WT neurons (Fig. S2D), suggesting that even low levels of mα-Syn levels are sufficient to attenuate inclusion formation.

hα-Syn inclusions reproduce key LB features and exhibit fibrillar ultrastructure

Several cellular models manifesting α-Syn accumulation into inclusions in human cell lines have been previously reported, either upon α-Syn over-expression alone(14-16), co-expression with synphilin-1(17),

exposure to proteasome inhibitors(9), or application of oxidative/nitrative insults(18, 19). Nevertheless, inclusions observed under these conditions typically don't reproduce all key LB features, including decreased solubility, hyper-phosphorylation at Serine-129 (pS129)(20), ubiquitination(21), Thioflavin-S binding, and fibrillar ultra-structural organization(1). Therefore, we assessed whether hα-Syn inclusions observed in *SNCA*$^{-/-}$ neurons fulfil these criteria.

To determine whether inclusion formation is linked with decreased hα-Syn solubility, WT or *SNCA*$^{-/-}$ neurons were infected with lentiviruses encoding hα-Syn and then fractionated into nonionic detergent-soluble and nonionic detergent-insoluble fractions. Using this assay, lentivirally infected *SNCA*$^{-/-}$ neurons showed significantly less monomeric hα-Syn in detergent-soluble fractions compared to WT counterparts (Fig. 1C). Interestingly, this effect was not due to decreased total hα-Syn expression in the *SNCA*$^{-/-}$ neurons, as similar total hα-Syn RNA and protein levels were observed in unfractionated WT and *SNCA*$^{-/-}$ neurons (Fig. S3A-B). In contrast, the decrease in soluble monomeric hα-Syn was concomitant with the appearance of high molecular weight (HMW) hα-Syn species in detergent-insoluble fractions of lentivirally infected *SNCA*$^{-/-}$ neurons (Fig. 1C). To validate our fractionation protocol, we treated control neurons with insoluble hα-Syn^{Alexa633} preformed fibrils (PFFs, characterized in Fig. S4), which showed strong signal almost exclusively within detergent-insoluble fractions as previously reported (Fig. 1C)(22). Altogether, these results suggest that abolishing mα-Syn expression enhances the aggregation propensity of hα-Syn in primary neurons, as reflected by decreased solubility and the formation of insoluble HMW aggregates.

One possibility is that the inclusions reflect aggregated hα-Syn that is contained within vesicles of the endo-lysosomal pathway. As such, we systematically assessed inclusion co-localization with specific markers for early endosomes (Rab5 and RhoB), late endosomes (Rab7), lysosomes (Lamp1), autophagosomes (LC3) and multi-lamellar bodies (CD63). As shown in Fig. S5, although some hα-Syn inclusions showed weak partial co-localization with co-transfected markers of late endosomes (Rab7-GFP) and lysosomes (Lamp1-RFP), indicating potential degradation by this pathway, most of the inclusions showed no colocalization with any of the transfected markers. As such, these findings rule out the possibility of all inclusions being merely vesicles of the endo-lysosomal pathway.

Next, we assessed whether the inclusions formed in *SNCA*$^{-/-}$ neurons are readily detectable using common LB probes; namely antibodies against α-Syn(1), pS129-α-Syn(20) and ubiquitin(21), as well as Thioflavin-S(23). As shown in Figure 1D, immuno-staining using nine different anti-α-Syn antibodies with epitopes spanning most of the α-Syn sequence all revealed bright spheroid intra-neuronal inclusions, thereby establishing that these structures indeed comprise hα-Syn which is not necessarily truncated at any of its termini. Moreover, dual immuno-fluorescence analysis showed that hα-Syn positive inclusions are

also hyper-phosphorylated at S129 and are ubiquitinated, and co-staining with Thioflavin-S indicated that the inclusions could comprise cross-β-sheet fibrillar content (Fig. 1E).

To establish whether the hα-Syn inclusions comprise fibrillar ultrastructure, we performed correlative light and electron microscopy (CLEM) analysis that allows ultra-structural examination of neurons previously identified by confocal microscopy as containing fluorescent inclusions (Fig. 2A-C). 72 hours (hrs) post-transfection, hα-Syn inclusions were detected in close association with nuclear and cytoplasmic membranes or near mitochondria, but were rarely found surrounded by a uniform lipid bilayer (Fig. 2B-C), thereby further ruling out the possibility of inclusions being vesicular in nature. Remarkably, high magnification ssTEM of the correlated inclusions revealed intertwining "whirls" of filamentous structures in most analyzed inclusions (Fig. 2B-C). Individual measurements of these structures showed that the filaments have an average diameter ranging between 7-13 nm (Fig. 2D), which is similar to that of fibrils within genuine LBs (24), thereby suggesting that hα-Syn could be aggregating into fibrils within these inclusions.

Alternatively, these observed "whirls" could represent membranous structures that have been entrapped within inclusions. To address this possibility, we performed an additional CLEM experiment where we treated neurons exhibiting *de novo* aggregates (composed of Myc-hα-Syn) with hα-Syn^{Alexa633} PFFs for 24 hrs, and compared within adjacent neurons, the ultrastructure and diameter of *de novo* filaments (comprising only Myc-hα-Syn) compared to internalized PFFs, mixtures of both, as well as to intracellular membranes. As shown in Figure S6, whereas intracellular membranes showed a broad diameter distribution ranging from 7-12 nm with a mean average of 8.7 nm, internalized PFFs and mixtures of *de novo* formed filaments and PFFs showed a much more defined width distribution of 10-13 nm and higher mean diameter of ~11 nm. Interestingly, although filaments in *de novo* inclusions exhibited a more broad width distribution than PFFs and mixtures being 7-13 nm, with some of the filaments having low diameter that could classify them as membranous, the vast majority (~75%) were in the range of 10-13 nm, which falls within the narrow distribution of PFFs and thereby supports their fibrillar nature.

To determine whether hα-Syn is the constituent of the observed fibrillar structures, we sought to assess their reactivity with antibodies against α-Syn by immuno-gold labelling. First, we probed the ability of four different antibodies (having different epitopes against the N-terminus, C-terminus and NAC region of α-Syn) to detect hα-Syn PFFs. Notably, we found that polyclonal anti-PAN-Syn antibodies such as the ab-6176 and FL-140 detect PFFs much more readily than monoclonal hα-Syn specific antibodies (Fig. S7). Therefore, we assessed the reactivity of the fibrillar structures observed within *SNCA*$^{-/-}$ neurons expressing hα-Syn to the ab-6176 antibody. Importantly, 3D reconstruction of ssTEM images clearly showed immuno-gold particles reacting with outer and inner portions of the whirls of filaments detected within inclusions

(Fig. 2E-F), thereby confirming Synuclein presence within these structures.

Altogether, these findings demonstrate that the inclusions observed in *SNCA*$^{-/-}$ neurons exhibit several similarities with LBs in terms of solubility and immuno-reactivity, and demonstrate signs of *bonafide* fibrillization events. However, the filaments do not have an orderly arrangement with a dense core as typically observed in brainstem LBs, but are embedded amongst an electron translucent medium, which is probably sequestered soluble α-Syn protein. As the filaments exhibit a disordered distribution, they may recapitulate early stages of LB formation, which may need more time or additional factors to mature and remodel into authentic LBs.

hα-Syn inclusions in *SNCA*$^{-/-}$ neurons grow in size and incorporate soluble α-Syn

We then investigated whether hα-Syn aggregation kinetics can be accurately evaluated in our novel neuronal model. In *SNCA*$^{-/-}$ neurons transiently expressing hα-Syn, inclusions were detected 24, 48 or 72 hrs post-transfection, and the size of inclusions appeared to increase over time as assessed by quantifying 3D-rendered inclusion volumes, with maximum size reached at 48 hrs post-transfection (Fig. 3A). To investigate the mechanisms underlying inclusion growth, we performed fluorescence live imaging experiments using hα-Syn that is N-terminally tagged to "mEOS2", a fluorescent protein that is photo-convertible from bright green (506 nm) to orange-red (584 nm) when excited at near-ultraviolet wavelengths(25). As shown in Figure 3B, somatic and neuritic mEOS2-α-Syn inclusions were detected 24 hrs post-transfection in *SNCA*$^{-/-}$ neurons, and these continued to grow in volume over 72 hrs. Moreover, the detected inclusions were reactive with antibodies against total α-Syn, ubiquitin, and pS129-α-Syn (Fig. 3C), thereby suggesting that the fusion protein reproduces the aggregation properties of untagged hα-Syn, and could be used to investigate the kinetics of this process in neurons.

Short interval (~1 hr) confocal live imaging followed by 3D surface rendering showed that the volume of individual inclusions increased over ~1 hr of imaging, with very few reversible fusion events noted (Fig. 3D). Moreover, analysis of the speed of moving particles showed that most detected inclusions are immobile (Fig. 3D), thereby ruling out the possibility of inclusion growth being mainly caused by fusion of small motile aggregates. Notably, the percent increase in volume was variable between different inclusions, with some doubling their volume within 50 minutes and others showing modest changes. This observation suggests that inclusion growth rate is not linear and constant over time, and is not necessarily similar for the whole population of inclusions within the same neuron.

To determine whether mEOS2-α-Syn inclusions incorporate soluble hα-Syn over time, we performed fluorescence recovery after photo-bleaching (FRAP) and photo-conversion live imaging experiments (Fig.

3E), which allow assessing rates of protein diffusion into (D_{IN}) and out-of (D_{OUT}) inclusions respectively, as well as determining the relative proportion of immobile protein within inclusions (immobile fraction, *IF*). In FRAP experiments, we photo-bleached individual inclusions and monitored the recovered fluorescence from diffusing soluble cytosolic protein. As shown in Figure 3F and Video S2, FRAP measurements displayed consistent recovery of fluorescent signal within photo-bleached inclusions, and mono-exponential fitting of FRAP plots from ~90 different inclusions allowed the estimation of D_{IN} and *IF*. The average value for D_{IN} was very low (~0.03 μm^2/sec), consistent with previous results for immobilized α-Syn-tetracystein inclusions in SH-SY5Y cells (0.03-0.04 μm^2/sec)(26), thereby suggesting the presence of a structure that impedes free diffusion. In line with this, ~32% of the protein was estimated to be found within the *IF*, thereby establishing that inclusions comprise immobilized proteins that are unable to equilibrate with the cytoplasmic pool, likely due to their binding to a dense compact structure. The presence of high amounts of soluble mobile protein (~68%) within inclusions is in line with our ssTEM data showing filamentous structures being embedded within a bulk of electron translucent *milieu*, which is most probably sequestered soluble protein.

In order to assess the D_{OUT}, we utilized the photo-convertible property of mEOS2, where we photo-converted individual inclusions by near-ultraviolet irradiation, and monitored the decrease in photo-converted fluorescence intensity within inclusions. The decay in fluorescence would reflect outward diffusion of proteins from the inclusions to the cytosol. As expected, irradiation of inclusions with a 405 nm laser successfully resulted in the photo-conversion of 488 nm mEOS2-α-Syn fluorescence to 568 nm (Fig. 3G and Video S3). Strikingly, whereas exponential fitting of decay curves from ~50 different neurons revealed a slightly lower estimation of the *IF* compared to that obtained from FRAP experiments (16 ±10%), the estimated D_{OUT} (0.0022 ±0.0007 μm^2/sec) was almost 16 folds lower than D_{IN} (Fig. 3H). This suggests that within the same time fraction, significantly more protein is going into inclusions compared to soluble protein that is diffusing out. As such, these findings together suggest that hα-Syn aggregates in *SNCA*$^{-/-}$ neurons incorporate soluble protein into highly stable structures, most likely the fibrils observed by ssTEM.

Inclusion formation in *SNCA*$^{-/-}$ neurons is an aggregation-driven process

To further establish whether hα-Syn inclusion formation is an aggregation-driven process, we assessed whether altering the aggregation propensity of hα-Syn affects formation and/or growth of neuronal inclusions. Two modified hα-Syn proteins, a C-terminally truncated variant (at position 120) that has been shown to aggregate more readily than full-length α-Syn *in vitro* and *in vivo*(27), and a variant with the S87E substitution that inhibits hα-Syn aggregation in similar models(28, 29) were expressed in WT or *SNCA*$^{-/-}$

neurons. As shown in Figure 4A, while similar proportions of *SNCA*$^{-/-}$ neurons expressing full-length (α-Syn^{FL}) or truncated (α-Syn$^{\Delta 120}$) hα-Syn developed inclusions, the S87E aggregation-deficient variant mostly exhibited diffuse distribution. This effect was not due to a difference in protein expression levels between the three proteins as similar mean fluorescence levels per neuron were detected across conditions (Fig. S8).

As that the α-Syn$^{\Delta 120}$ mutant could be affecting the size of individual aggregates, we investigated kinetics of mEOS-α-Syn inclusion growth by live imaging (Fig. 4B-C). Surface reconstruction of inclusions in 50 neurons per condition showed that mEOS2-α-Syn$^{\Delta 120}$ forms significantly larger inclusions 24 hrs post-transfection compared to mEOS2-α-Syn^{WT} (Fig. 4C). In contrast, the few inclusions formed by the mEOS2-α-Syn^{S87E} mutant were much smaller at 48 hrs (Fig. 4C). In a complementary strategy, we investigated whether treatment with a pharmacological aggregation inhibitor "Tolcapone"(30) would affect inclusion formation in this model. Remarkably, Tolcapone treatment reduced inclusion formation by ~60% and restored the diffuse distribution of hα-Syn in *SNCA*$^{-/-}$ neurons (Fig. 4D). As such, these results together demonstrate that inclusion formation in *SNCA*$^{-/-}$ neurons is aggregation-driven, as introducing a single amino-acid substitution known to inhibit hα-Syn aggregation propensity or treatment with a known aggregation inhibitor significantly attenuate inclusion formation.

Endogenous β-Syn KO is a natural hα-Syn aggregation inhibitor in neurons

An attractive general implication of our findings is that homologous members of the synuclein family could naturally act as physiological inhibitors of abnormal α-Syn aggregation. Therefore, we assessed whether the other members of the synuclein family, β-Syn and γ-Syn, exert a similar inhibitory effect on hα-Syn aggregation. To test this, we prepared neuronal cultures from mice lacking β-Syn (β-Syn KO)(31), γ-Syn (γ-Syn KO)(32), or all three synucleins (triple KO)(33). Loss of α- and β-Syn in corresponding KO cultures was validated by immunocytochemistry (Fig. 5A), and γ-Syn expression was not detectable in any of the cultures, probably due to its low expression levels in hippocampal neurons as previously reported(34). Remarkably, when we assessed the distribution of exogenously expressed hα-Syn across the different cultures (Fig. 5B), we found that β-Syn KO and triple KO neurons similarly develop LB-like inclusions, unlike WT controls and γ-Syn KO neurons that mostly exhibit diffuse hα-Syn distribution. Importantly, the inclusions formed in β-Syn KO and triple KO neurons were also hyper-phosphorylated at S129, hence exhibiting a key pathological LB-like phenotype (Fig. 5C). These findings suggest that unlike endogenous γ-Syn, the other two homologues α-Syn and β-Syn have similar inhibitory effects on ectopic hα-Syn aggregation. Importantly however, as similar percentages of β-Syn KO and triple KO neurons develop

inclusions (~35%), this intriguingly rules out the presence of a synergistic effect for the deletion of both proteins.

The absence of mα-Syn promotes specific aggregation of hα-Syn *in vivo*

To test whether the presence of mα-Syn affects the aggregation propensity of hα-Syn in the brain, we generated mice lacking endogenous mα-Syn (*SNCA*$^{-/-}$)(13) and carrying two copies of hα-Syn(*hα-Syn*$^{+/+}$)(35) (Fig. S9A). Biochemical fractionation of brain homogenates into cytosolic (soluble) and particulate (insoluble) protein fractions was performed to assess whether these mice (*hα-Syn*$^{+/+}$*SNCA*$^{-/-}$) exhibit changes in hα-Syn aggregation and solubility, compared to *hα-Syn*$^{+/+}$ controls expressing endogenous mα-Syn. In line with our previous data, less monomeric hα-Syn was detected in soluble fractions derived from *hα-Syn*$^{+/+}$*SNCA*$^{-/-}$ mice compared to *hα-Syn*$^{+/+}$ counterparts (Fig. 6A). This decrease in monomeric hα-Syn was concomitant with the appearance of HMW hα-Syn species within insoluble fractions, which were detected using three different antibodies against hα-Syn thereby establishing their specificity (Fig. 6A, Fig. S9B). Moreover, the decrease in soluble hα-Syn was not due to decreased total hα-Syn expression in *hα-Syn*$^{+/+}$*SNCA*$^{-/-}$ mice compared to *hα-Syn*$^{+/+}$ counterparts, as similar total hα-Syn mRNA and protein levels were observed in unfractionated brains of both genotypes (Fig. S9C-D). As such, these findings altogether suggest that hα-Syn is readily aggregating and becoming less soluble in the absence of mα-Syn in Tg mouse brains.

To further evaluate the extent of *in vivo* hα-Syn aggregation, we performed immuno-histochemical analyses on sections treated with proteinase-K, which allows selective visualization of resistant aggregates. Consistent with previous studies (35), *hα-Syn*$^{+/+}$ mice showed abundant intra-neuronal α-Syn immunoreactive inclusions in the cortex, of which some were proteinase-K resistant (Fig. 6B). Strikingly, cortical and striatal neurons from *hα-Syn*$^{+/+}$*SNCA*$^{-/-}$ mice showed higher immunoreactivity to anti-α-Syn antibodies and exhibited a significant increase in proteinase-K resistant inclusions in the cortex and hippocampus (Fig. 6B). Moreover, double immuno-labelling experiments showed that inclusions are phosphorylated at S129, and exhibit strong reactivity for the synaptic vesicle protein synaptophysin (Fig. 6C-D), both of which being markers of LB pathology (20, 36). Taken together, these findings demonstrate that the aggregation propensity of hα-Syn is enhanced in the absence of mα-Syn *in vivo*, as reflected by decreased solubility and accumulation of hα-Syn into proteinase-K resistant inclusions.

To assess whether abolishing of mα-Syn expression would promote the aggregation of human β-synuclein (hβ-Syn), the considerably less aggregation prone homologue of hα-Syn, we crossed transgenic mice expressing hβ-Syn(37) with mα-Syn null mice to generate *hβ-Syn*$^{+/+}$*SNCA*$^{-/-}$ transgenics. Biochemical

fractionation revealed that in contrast to the promotion of hα-Syn aggregation, the absence of mα-Syn did not affect the levels of soluble hβ-Syn or cause the appearance of insoluble hβ-Syn species (Fig. S10A). In addition, immuno-histochemical analysis showed that hβ-Syn was mostly localized within neuronal terminals and did not show any inclusions neither in brains of *hβ-Syn*$^{+/+}$ mice as previously reported (37), nor in brains of *hβ-Syn*$^{+/+}$*SNCA*$^{-/-}$ mice (Fig. S10B). As such, these results show that α-Syn ablation does not promote the aggregation of hβ-Syn *in vivo*, thereby conferring specificity to the effect we observe in *hα-Syn*$^{+/+}$*SNCA*$^{-/-}$ mice.

mα-Syn interacts with aggregated hα-Syn species attenuating seeding and spreading

To investigate the mechanism *via* which mα-Syn affects hα-Syn aggregation, we first assessed whether over-expressed hα-Syn directly interacts with endogenous mα-Syn in WT primary neurons. Notably, we did not detect any interaction between the two proteins at the monomer level by co-immuno-precipitation (Fig. S11A). To investigate whether mα-Syn interacts with multimeric/aggregated hα-Syn species rather than hα-Syn monomers, we assessed the interaction of mα-Syn monomers with equimolar amounts of hα-Syn monomers or hα-Syn sonicated fibrils (PFFs; characterized in Fig. S12). Intriguingly, mα-Syn was co-immuno-precipitated only when it was mixed with hα-Syn PFFs and not the hα-Syn monomers (Fig. 7A), indicating that monomeric mα-Syn preferentially interacts with hα-Syn PFFs *in vitro*. In order to confirm these findings and to obtain a quantitative assessment of the interaction between mα-Syn monomers and hα-Syn PFFs by an independent readout, we performed surface plasmon resonance (SPR) measurements. Briefly, saturating amounts of either hα-Syn monomers or hα-Syn PFFs were immobilized by amine coupling to separate CM5 chips, and then increasing concentrations of mα-Syn monomers were flushed on to the chips. As shown in Figure 7B, and in line with our immuno-precipitation experiments, no interaction was noted between injected mα-Syn monomers and immobilized hα-Syn monomers, even at the highest tested concentration for mα-Syn (10 μM). In contrast, mα-Syn monomers readily interacted with hα-Syn sonicated PFFs in a dose dependent manner, even at concentrations as low as 0.1 μM.

To investigate whether endogenous mα-Syn similarly interacts with aggregated hα-Syn species in primary neurons, we treated WT neurons with sonicated hα-Syn PFFs and assessed interaction by immuno-precipitation and immuno-fluorescence analyses. Importantly, and in line with our *in vitro* results, mα-Syn co-immuno-precipitated with pulled down hα-Syn PFFs (Fig. S11B). Moreover, confocal imaging revealed that internalized hα-Syn PFFs colocalize with endogenous mα-Syn (Fig. S11C), which radically redistributes from diffuse somatic localization into defined puncta as previously described (22). Altogether, these results show that mα-Syn preferentially interacts with aggregated hα-Syn PFFs *in vitro* and in neurons.

Next, we explored whether such an interaction between α-Syn PFFs and α-Syn monomers from different species would seed or alternatively attenuate progressive monomer aggregation. As such, we assessed aggregation kinetics of hα-Syn or mα-Syn monomers in the presence of either hα-Syn PFFs or mα-Syn PFFs (characterized in Fig. S12). Strikingly, assessment of Thioflavin-T binding, remaining monomer content and fibrillar morphology by electron microscopy all consistently showed that the fibrillization α-Syn monomers is predominantly accelerated (seeded) in the presence of α-Syn PFFs of the same species. For instance, whereas the lag phase was eliminated in the mixture of hα-Syn monomers and hα-Syn PFFs resulting in the appearance of fibrillar structures as of 8 hrs of incubation (Fig. 7C-F), the aggregation kinetic of the mixture of hα-Syn monomers and mα-Syn PFFs was similar to that of hα-Syn alone, where only oligomeric species were formed at 8 hrs of incubation. Similar observations were noted for the mixture mα-Syn monomers and mα-Syn PFFs, which showed the most dramatic elimination of the lag phase, and formation of fibrils after only 2 hrs of incubation (Fig. S13A-D). Here again, the addition of hα-Syn PFFs to mα-Syn monomers failed to promote aggregation to a similar extent, only forming oligomeric species at 2 hrs. Altogether, these findings strongly show that α-Syn aggregation kinetics are significantly accelerated when the seeds and monomers are from the same species, and that the presence of mixed species of monomers and PFFs results in in less seeding propensity and slower aggregation kinetics.

To evaluate whether the seeding and spreading potential of α-Syn PFFs is similarly affected upon having PFFs and endogenous monomers of the same species in the brain, we injected either mα-Syn PFFs or hα-Syn PFFs into the striatum of WT (non-transgenic) or *SNCA*$^{-/-}$ mice (as controls), and then compared the seeding and spreading propensity in different brain regions one month post-injection. Strikingly, we observed most pronounced spreading α-Syn pathology when mα-Syn PFFs were injected into WT mice expressing endogenous mα-Syn (Fig. 8G), as mα-Syn accumulated into somatic inclusions that are ubiquitinated and hyperphosphorylated at S129 in the cortex and amygdala (Fig. S13E). In contrast, hα-Syn PFFs induced significantly less pathology at these regions in WT mice at the same time-point. Moreover, *SNCA*$^{-/-}$ mice showed very limited overall pathology following injection with either hα-Syn PFFs or mα-Syn PFFs, indicating that the observed inclusions in WT mice injected with mα-Syn PFFs reflect the seeding and propagation of endogenous mα-Syn. Altogether, these findings show that *in vitro* and *in vivo*, α-Syn PFFs preferentially seed the aggregation of monomeric α-Syn of the same species, and therefore, the interaction of monomers and PFFs from different species does not promote progressive seeding and spreading of pathology.

Discussion

The aggregation of α-Syn into LBs has been directly linked to the pathogenesis of PD(2). The mechanism of formation and the precise effect of LBs on neuronal physiology and viability remains poorly understood, mostly due to the lack of animal and cellular models exhibiting *de novo* α-Syn fibrillization into authentic LB-like structures. Although doubling α-Syn expression is sufficient to cause PD in humans, attempts to reproduce molecular PD pathology based on α-Syn over-expression in various animal models have not been successful. This could imply the presence of cellular factors that inhibit hα-Syn aggregation in these models. In this study, we sought to systematically examine whether endogenous α-Syn homologues attenuate hα-Syn aggregation in neurons. Using different Synuclein KO cultures, we found that a substantial fraction of *SNCA*$^{-/-}$ neurons expressing hα-Syn develop inclusions that exhibit key LB-like features, including S129 hyper-phosphorylation, ubiquitination and Thioflavin-S reactivity. Importantly, this phenomenon reflected *de novo* hα-Syn fibrillization as revealed by ssTEM following both CLEM and immuno-gold labelling experiments. To the best of our knowledge, these features have not been altogether reported in any of the previously published cellular models that rely on the sole over-expression of hα-Syn.

Multiple lines of evidence from many of our experiments further converged to establish that inclusion formation *SNCA*$^{-/-}$ neurons is an aggregation driven process. Over-expression of the aggregation incompetent mutant S87E or treatment with the pharmacological aggregation inhibitor "Tolcapone" resulted in marked reduction in inclusion formation. In contrast, overexpression of the aggregation-prone truncated hα-Syn variant (1-120) resulted in the formation of larger inclusions compared to the WT protein. In all cases where we observed increased inclusion formation, we also observed decreased hα-Syn solubility and the appearance of HMW aggregates, concomitant with the loss of monomers. Moreover, time-lapse live imaging coupled with FRAP and photo-conversion experiments showed in real time that the inclusions grow in size and readily incorporate soluble hα-Syn protein. Interestingly however, when we explored the toxic potential of these inclusions, we found that the aggregates formed do not provoke increased toxicity (SI Text, Fig. S14-15), consistent with previous studies suggesting that intracellular hα-Syn aggregates may be protective in cellular models (38, 39).

Having established that *SNCA*$^{-/-}$ primary neurons are more permissive for hα-Syn aggregation in culture, we sought to validate this finding *in vivo*. Two previous independent studies had suggested that expression of hα-Syn$^{\Delta 120}$ or hα-Syn^{A53T} in Tg mice lacking mα-Syn expression leads to the formation of fibrillar inclusions within the *Substantia nigra* or spinal cord respectively(5, 6). Therefore, we directly compared the aggregation propensity of Tg hα-Syn in brains of mice expressing mα-Syn(35), or having no endogenous mα-Syn expression. Our data showed that hα-Syn exhibits enhanced aggregation propensity in the absence of mα-Syn, which was reflected by decreased solubility, enhanced detection of HMW oligomeric species, and formation of abundant proteinase-K resistant and pS129 hyper-phosphorylated

inclusions. In order to rule out the possibility that knocking out mα-Syn promotes nonspecific aggregation, we conducted similar studies on hβ-Syn, an α-Syn homologue which is significantly less prone to aggregate. As expected, knocking out mα-Syn did not affect the levels, distribution or staining pattern of hβ-Syn in transgenic mice.

Our observation that the re-introduction of mα-Syn in *SNCA*$^{-/-}$ neurons significantly attenuates hα-Syn inclusion formation suggests that the mouse homologue could be directly inhibiting hα-Syn aggregation. Intriguingly, although we could not detect prominent interaction between human and mα-Syn at the monomeric level in neurons, we consistently observed that mα-Syn preferentially interacts with sonicated PFFs *in vitro,* and in neurons. Moreover, we found that this interaction does not promote progressive seeding and spreading of pathology *in vitro* or in mouse brains *in vivo*. As such, endogenous mα-Syn could be directly inhibiting hα-Syn fibrillization in WT primary neurons by stabilizing oligomeric species and capping terminals of early fibrillar stretches formed by hα-Syn (Fig. 7H).This proposition is well in line with the previous study by Rochet et al.(7) showing that *in vitro*, mα-Syn inhibits the fibrillization of hα-Syn by stabilizing oligomers on the pathway to amyloid formation. Moreover, it is consistent with literature reports which imply that the propagation and spreading of α-Syn pathology is prominent under conditions where the injected PFFs and host expressed monomers are from the same species. In most of these studies, seeding and spreading of α-Syn pathology was observed when mα-Syn PFFs was injected in non-transgenic mice expressing mα-Syn (40-42), or when hα-Syn PFFs were injected into transgenic mice expressing human α-Syn protein (43-48).

An attractive general implication of our findings is that aggregation attenuation by homologous proteins could represent a generic biological phenomenon. This proposition is in harmony with multiple studies reporting decreased aggregation kinetics in the presence of amyloidogenic homologous proteins underlying different diseases. For instance, the key peptides involved in the formation of amyloid plaques in Alzheimer's disease, Aβ40 and Aβ42, were shown to reciprocally inhibit each other's aggregation *in vitro* in a concentration dependent manner(49). Moreover, mutant hemoglobin β-chain polymerization in sickle cell anemia was shown to be attenuated upon increasing ratios of its γ-chain homologue(50). Likewise, in transthyretin (TTR) amyloid diseases, murine/human TTR homologues form hetero-tetramers that impair amyloid formation(51, 52), and aggregation *in vivo* was achieved mostly in Tg mice expressing TTR mutants on an endogenous TTR KO background(52). Finally, the aggregation kinetics of the "islet amyloid polypeptide" (IAPP) in bulk solution were shown to be dramatically affected by the presence of its rat homologue (53, 54).

In light of all these findings, we investigated whether this phenomenon could be extended to the other endogenous hα-Syn homologues; β-Syn and γ-Syn. Interestingly, we found that β-Syn KO cultures also

developed hα-Syn inclusions that were hyper-phosphorylated as S129. In contrast, the distribution of hα-Syn was not affected when expressed in γ-Syn KO neurons, which was expected because γ-Syn levels in WT hippocampal neurons were already very low, and therefore could not be drastically reduced in γ-Syn KO neurons. These results are also in line with previous reports showing that β-Syn inhibits α-Syn aggregation *in vitro*(55, 56), as well as *in vivo*, as double transgenic mice co-expressing both human α- and β-Syn exhibit ameliorated motor deficits and lower α-Syn accumulation(37, 57). Our results however further suggest that the total levels or ratio of both endogenous α- and β-Syn could be critical in protecting against hα-Syn aggregation. Once this level drops below a certain threshold (either in the single or triple KOs), aggregation of hα-Syn into LB-like inclusions becomes progressive. Supporting this proposition is the observation that intermediate reduction of mα-Syn levels by shRNA did not promote hα-Syn inclusion formation in WT neurons.

In summary, we have shown that two endogenous members of the synuclein family, mα-Syn and mβ-Syn, attenuate the aggregation of over-expressed hα-Syn in mouse neurons. Taken together with the multitude of studies that have reported aggregation inhibition in the presence of amyloidogenic homologous proteins (such as Aβ, TTR, Haemoglobin and IAPP), this observation could reflect a more generic biological phenomenon, where endogenous homologues act as natural inhibitors of abnormal aggregation. Not only could this explain why most current rodent PD models relying on hα-Syn overexpression in WT mice do not show prominent hα-Syn fibrillization, but it also provides novel cellular and *in vivo* models that reproduce for the first time, the clear formation of fibrillar hα-Syn aggregates. The ability to quantitatively assess the dynamics of inclusion formation in these models provides unique opportunities to elucidate molecular and cellular determinants that influence the mechanisms of α-Syn fibrillization in living neurons, and the identification of pathways that modulate this process and contribute to neurodegeneration. Further studies using these models could allow identifying novel drugs for the treatment of PD based on modulating α-Syn aggregation and inter-neuronal spreading, or enhancing the degradation and clearance of toxic α-Syn aggregates.

Materials and Methods

Further experimental details are provided in *SI Text*.

Primary neuron culture preparation, transfection, infection and Tolcapone treatment. Primary hippocampal neuronal cultures were prepared from P0 C57BL/6JRccHsd (WT, Harlan laboratories), C57BL/6JOlaHsd (α-Syn KO, Harlan laboratories)(12), B6,129X1-*Snca*^{tm1Rosl}/J (α-Syn KO, Jackson

laboratories)(13), β-Syn KO(31), γ-Syn KO(58), or α-β-γ-Syn KO mice(33) as previously described(10). Briefly, hippocampi were dissociated with papain and triturated using a glass pipette. After centrifugation at 400 *g* for 2 min, cells were plated in MEM/10% horse serum onto poly-L-lysine (Sigma) coated coverslips (glass 12mm, VWR, for immunocytochemistry; or thermanox plastic 13mm, Nunc, for TEM) at 1.5×10^5 cells/ml, or at 3×10^5 cells/ml in 35mm confocal dishes (World Precision, for live imaging) or in 10 cm dishes (BD Biosciences, for biochemical analysis). Medium was changed after 4 hrs to Neurobasal/ B27 medium, and neurons were treated with ARAC (Sigma) after 6 days-in-vitro (DIV) to stop glial division. At 7 DIV, neurons were either transiently transfected using Lipofectamine™ 2000 (Invitrogen) according to manufacturer's instructions for up to 3 days, or infected with lentiviruses at a multiplicity of infection of 10 for up to 7 days. When indicated, 24 hrs post-transfection, neurons were treated with 20 μM Tolcapone (Sigma) for an additional 24 hrs before immunocytochemistry.

Acknowledgments

We thank Nathalie Jordan, John Perrin and Celine Vocat for help in preparing primary cultures, plasmid cloning, and production of recombinant proteins. We also thank Prof. Virginia Lee for kindly providing the Syn-208 antibody, Mr. Samuel Kilchenmann for expert help in conducting and analyzing SPR experiments, Dr. Anne-Laure Mahul and Dr. Issa Issac for helping with blinded quantification of some experiments, Mr. Maroun Bou Sleiman for help with statistical analysis and Dr. Juan Reyes for critically evaluating the manuscript. This work was supported by the Swiss Federal Institute of Technology, the Swiss National Science Foundation and the Wellcome Trust Grant (075615/Z/04/z) to VLB.

References

1. Spillantini MG*, et al.* (1997) Alpha-synuclein in Lewy bodies. *Nature* 388(6645):839-840.
2. Lashuel HA, Overk CR, Oueslati A, & Masliah E (2013) The many faces of alpha-synuclein: from structure and toxicity to therapeutic target. *Nat Rev Neurosci* 14(1):38-48.
3. Dawson TM, Ko HS, & Dawson VL (2010) Genetic animal models of Parkinson's disease. *Neuron* 66(5):646-661.
4. Feany MB & Bender WW (2000) A Drosophila model of Parkinson's disease. *Nature* 404(6776):394-398.
5. Cabin DE*, et al.* (2005) Exacerbated synucleinopathy in mice expressing A53T SNCA on a Snca null background. *Neurobiol Aging* 26(1):25-35.
6. Tofaris GK*, et al.* (2006) Pathological changes in dopaminergic nerve cells of the substantia nigra and olfactory bulb in mice transgenic for truncated human alpha-synuclein(1-120): implications for Lewy body disorders. *J Neurosci* 26(15):3942-3950.
7. Rochet JC, Conway KA, & Lansbury PT, Jr. (2000) Inhibition of fibrillization and accumulation of prefibrillar oligomers in mixtures of human and mouse alpha-synuclein. *Biochemistry* 39(35):10619-10626.
8. Petrucelli L*, et al.* (2002) Parkin protects against the toxicity associated with mutant alpha-synuclein: proteasome dysfunction selectively affects catecholaminergic neurons. *Neuron* 36(6):1007-1019.
9. McLean PJ, Kawamata H, & Hyman BT (2001) Alpha-synuclein-enhanced green fluorescent protein fusion proteins form proteasome sensitive inclusions in primary neurons. *Neuroscience* 104(3):901-912.
10. Fares MB*, et al.* (2014) The novel Parkinson's disease linked mutation G51D attenuates in vitro aggregation and membrane binding of alpha-synuclein, and enhances its secretion and nuclear localization in cells. *Hum Mol Genet*.
11. Khalaf O*, et al.* (2014) The H50Q mutation enhances alpha-synuclein aggregation, secretion, and toxicity. *J Biol Chem* 289(32):21856-21876.
12. Specht CG & Schoepfer R (2001) Deletion of the alpha-synuclein locus in a subpopulation of C57BL/6J inbred mice. *BMC Neurosci* 2:11.
13. Abeliovich A*, et al.* (2000) Mice lacking alpha-synuclein display functional deficits in the nigrostriatal dopamine system. *Neuron* 25(1):239-252.
14. Tabrizi SJ*, et al.* (2000) Expression of mutant alpha-synuclein causes increased susceptibility to dopamine toxicity. *Hum Mol Genet* 9(18):2683-2689.
15. Opazo F, Krenz A, Heermann S, Schulz JB, & Falkenburger BH (2008) Accumulation and clearance of alpha-synuclein aggregates demonstrated by time-lapse imaging. *J Neurochem* 106(2):529-540.

16. Tofaris GK, Layfield R, & Spillantini MG (2001) alpha-synuclein metabolism and aggregation is linked to ubiquitin-independent degradation by the proteasome. *FEBS Lett* 509(1):22-26.
17. Engelender S*, et al.* (1999) Synphilin-1 associates with alpha-synuclein and promotes the formation of cytosolic inclusions. *Nat Genet* 22(1):110-114.
18. Lee HJ, Shin SY, Choi C, Lee YH, & Lee SJ (2002) Formation and removal of alpha-synuclein aggregates in cells exposed to mitochondrial inhibitors. *J Biol Chem* 277(7):5411-5417.
19. Paxinou E*, et al.* (2001) Induction of alpha-synuclein aggregation by intracellular nitrative insult. *J Neurosci* 21(20):8053-8061.
20. Fujiwara H*, et al.* (2002) alpha-Synuclein is phosphorylated in synucleinopathy lesions. *Nat Cell Biol* 4(2):160-164.
21. Hasegawa M*, et al.* (2002) Phosphorylated alpha-synuclein is ubiquitinated in alpha-synucleinopathy lesions. *J Biol Chem* 277(50):49071-49076.
22. Volpicelli-Daley LA*, et al.* (2011) Exogenous alpha-synuclein fibrils induce Lewy body pathology leading to synaptic dysfunction and neuron death. *Neuron* 72(1):57-71.
23. Irwin DJ, Lee VM, & Trojanowski JQ (2013) Parkinson's disease dementia: convergence of alpha-synuclein, tau and amyloid-beta pathologies. *Nat Rev Neurosci* 14(9):626-636.
24. Spillantini MG, Crowther RA, Jakes R, Hasegawa M, & Goedert M (1998) alpha-Synuclein in filamentous inclusions of Lewy bodies from Parkinson's disease and dementia with lewy bodies. *Proc Natl Acad Sci U S A* 95(11):6469-6473.
25. McKinney SA, Murphy CS, Hazelwood KL, Davidson MW, & Looger LL (2009) A bright and photostable photoconvertible fluorescent protein. *Nat Methods* 6(2):131-133.
26. Roberti MJ, Jovin TM, & Jares-Erijman E (2011) Confocal fluorescence anisotropy and FRAP imaging of alpha-synuclein amyloid aggregates in living cells. *PLoS One* 6(8):e23338.
27. Oueslati A, Fournier M, & Lashuel HA (2010) Role of post-translational modifications in modulating the structure, function and toxicity of alpha-synuclein: implications for Parkinson's disease pathogenesis and therapies. *Prog Brain Res* 183:115-145.
28. Paleologou KE*, et al.* (2010) Phosphorylation at S87 is enhanced in synucleinopathies, inhibits alpha-synuclein oligomerization, and influences synuclein-membrane interactions. *J Neurosci* 30(9):3184-3198.
29. Oueslati A, Paleologou KE, Schneider BL, Aebischer P, & Lashuel HA (2012) Mimicking phosphorylation at serine 87 inhibits the aggregation of human alpha-synuclein and protects against its toxicity in a rat model of Parkinson's disease. *J Neurosci* 32(5):1536-1544.
30. Di Giovanni S*, et al.* (2010) Entacapone and tolcapone, two catechol O-methyltransferase inhibitors, block fibril formation of alpha-synuclein and beta-amyloid and protect against amyloid-induced toxicity. *J Biol Chem* 285(20):14941-14954.
31. Chandra S*, et al.* (2004) Double-knockout mice for alpha- and beta-synucleins: effect on synaptic functions. *Proc Natl Acad Sci U S A* 101(41):14966-14971.
32. Buchman VL*, et al.* (1998) Persyn, a member of the synuclein family, has a distinct pattern of expression in the developing nervous system. *J Neurosci* 18(22):9335-9341.
33. Anwar S*, et al.* (2011) Functional alterations to the nigrostriatal system in mice lacking all three members of the synuclein family. *J Neurosci* 31(20):7264-7274.
34. Li J, Henning Jensen P, & Dahlstrom A (2002) Differential localization of alpha-, beta- and gamma-synucleins in the rat CNS. *Neuroscience* 113(2):463-478.
35. Masliah E*, et al.* (2000) Dopaminergic loss and inclusion body formation in alpha-synuclein mice: implications for neurodegenerative disorders. *Science* 287(5456):1265-1269.
36. Nishimura M*, et al.* (1994) Synaptophysin and chromogranin A immunoreactivities of Lewy bodies in Parkinson's disease brains. *Brain Res* 634(2):339-344.

37. Hashimoto M, Rockenstein E, Mante M, Mallory M, & Masliah E (2001) beta-Synuclein inhibits alpha-synuclein aggregation: a possible role as an anti-parkinsonian factor. *Neuron* 32(2):213-223.
38. Ko LW, Ko HH, Lin WL, Kulathingal JG, & Yen SH (2008) Aggregates assembled from overexpression of wild-type alpha-synuclein are not toxic to human neuronal cells. *J Neuropathol Exp Neurol* 67(11):1084-1096.
39. Tanaka M, *et al.* (2004) Aggresomes formed by alpha-synuclein and synphilin-1 are cytoprotective. *J Biol Chem* 279(6):4625-4631.
40. Luk KC, *et al.* (2012) Pathological alpha-synuclein transmission initiates Parkinson-like neurodegeneration in nontransgenic mice. *Science* 338(6109):949-953.
41. Masuda-Suzukake M, *et al.* (2014) Pathological alpha-synuclein propagates through neural networks. *Acta neuropathologica communications* 2:88.
42. Paumier KL, *et al.* (2015) Intrastriatal injection of pre-formed mouse alpha-synuclein fibrils into rats triggers alpha-synuclein pathology and bilateral nigrostriatal degeneration. *Neurobiol Dis* 82:185-199.
43. Betemps D, *et al.* (2014) Alpha-synuclein spreading in M83 mice brain revealed by detection of pathological alpha-synuclein by enhanced ELISA. *Acta neuropathologica communications* 2:29.
44. Luk KC, *et al.* (2012) Intracerebral inoculation of pathological alpha-synuclein initiates a rapidly progressive neurodegenerative alpha-synucleinopathy in mice. *J Exp Med* 209(5):975-986.
45. Sacino AN, *et al.* (2014) Brain injection of alpha-synuclein induces multiple proteinopathies, gliosis, and a neuronal injury marker. *J Neurosci* 34(37):12368-12378.
46. Peelaerts W, *et al.* (2015) alpha-Synuclein strains cause distinct synucleinopathies after local and systemic administration. *Nature* 522(7556):340-344.
47. Sacino AN, *et al.* (2014) Intramuscular injection of alpha-synuclein induces CNS alpha-synuclein pathology and a rapid-onset motor phenotype in transgenic mice. *Proc Natl Acad Sci U S A* 111(29):10732-10737.
48. Sacino AN, *et al.* (2013) Induction of CNS alpha-synuclein pathology by fibrillar and non-amyloidogenic recombinant alpha-synuclein. *Acta neuropathologica communications* 1(1):38.
49. Hasegawa K, Yamaguchi I, Omata S, Gejyo F, & Naiki H (1999) Interaction between A beta(1-42) and A beta(1-40) in Alzheimer's beta-amyloid fibril formation in vitro. *Biochemistry* 38(47):15514-15521.
50. Eaton WA & Hofrichter J (1995) The biophysics of sickle cell hydroxyurea therapy. *Science* 268(5214):1142-1143.
51. Hammarstrom P, Schneider F, & Kelly JW (2001) Trans-suppression of misfolding in an amyloid disease. *Science* 293(5539):2459-2462.
52. Sousa MM, *et al.* (2002) Evidence for early cytotoxic aggregates in transgenic mice for human transthyretin Leu55Pro. *Am J Pathol* 161(5):1935-1948.
53. Cao P, Meng F, Abedini A, & Raleigh DP (2010) The ability of rodent islet amyloid polypeptide to inhibit amyloid formation by human islet amyloid polypeptide has important implications for the mechanism of amyloid formation and the design of inhibitors. *Biochemistry* 49(5):872-881.
54. Sellin D, Yan LM, Kapurniotu A, & Winter R (2010) Suppression of IAPP fibrillation at anionic lipid membranes via IAPP-derived amyloid inhibitors and insulin. *Biophys Chem* 150(1-3):73-79.
55. Uversky VN, *et al.* (2002) Biophysical properties of the synucleins and their propensities to fibrillate: inhibition of alpha-synuclein assembly by beta- and gamma-synucleins. *J Biol Chem* 277(14):11970-11978.
56. Park JY & Lansbury PT, Jr. (2003) Beta-synuclein inhibits formation of alpha-synuclein protofibrils: a possible therapeutic strategy against Parkinson's disease. *Biochemistry* 42(13):3696-3700.
57. Fan Y, *et al.* (2006) Beta-synuclein modulates alpha-synuclein neurotoxicity by reducing alpha-synuclein protein expression. *Hum Mol Genet* 15(20):3002-3011.

58. Robertson DC, *et al.* (2004) Developmental loss and resistance to MPTP toxicity of dopaminergic neurones in substantia nigra pars compacta of gamma-synuclein, alpha-synuclein and double alpha/gamma-synuclein null mutant mice. *J Neurochem* 89(5):1126-1136.

Figures and legends

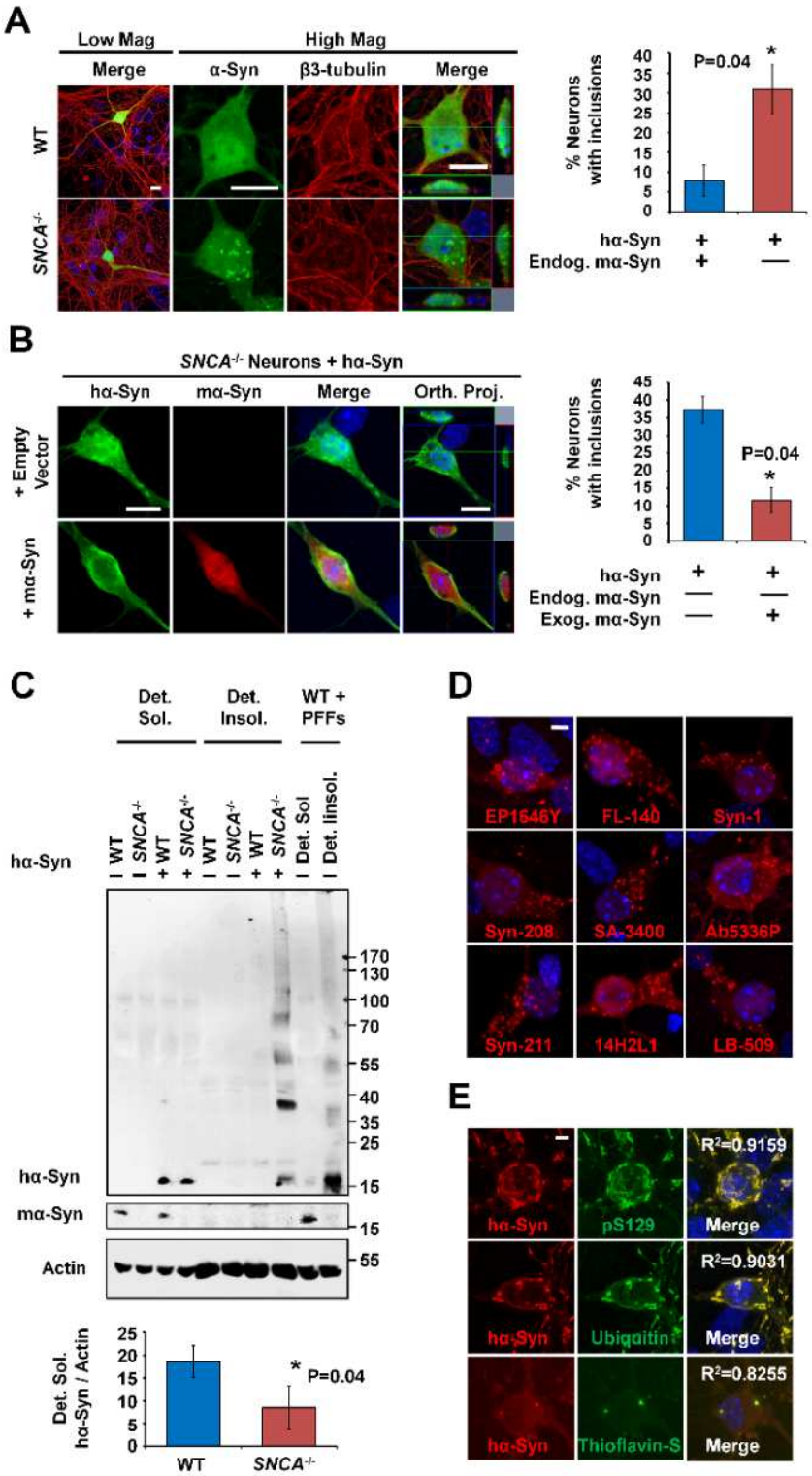

Fig. 1. The absence of mα-Syn promotes hα-Syn aggregation in primary neurons. (**A**) hα-Syn exhibits diffuse distribution in WT transfected neurons, and forms inclusions in cell bodies and neurites of *SNCA*$^{-/-}$ neurons. Orthogonal Z-stack projections are shown to verify the intra-cellular nature of inclusions.

Quantification of 25 neurons per condition (n=3 independent experiments) shows that significantly more *SNCA*$^{-/-}$ neurons develop inclusions (>1 µm in diameter). β3 tubulin staining was performed to reveal neurons. **(B)** Overexpressed hα-Syn reassumes its diffuse localization in *SNCA*$^{-/-}$ neurons upon restoring mα-Syn expression by transient transfection. Quantification of inclusion formation (>1µm) in 25 neurons per condition (n=3 independent experiments) shows significantly less inclusions formation in *SNCA*$^{-/-}$ neurons co-expressing both proteins. **(C)** Less monomeric hα-Syn is detected in nonionic detergent-soluble (Det. Sol.) fractions of lentivirally infected *SNCA*$^{-/-}$ neurons compared to WT counterparts. In contrast, nonionic detergent-insoluble (Det. Insol.) fractions of infected *SNCA*$^{-/-}$ neurons show more monomeric and HMW hα-Syn species, comparably to Det. Insol. fractions of WT neurons treated for 3 days with hα-Syn PFFs (0.5 µM). Actin was used to control for equal protein loading. Densitometric quantification (n=4 independent experiments) of Det. Sol. hα-Syn reveals significantly decreased levels when expressed in *SNCA*$^{-/-}$ compared to WT neurons. In "A-C", the Mann-Whiney test was applied to obtain P values (overlayed on histograms showing mean ± standard deviation (SD)). In "B-C", hα-Syn and mα-Syn were differentially revealed using the Syn-211 and D37A6 antibodies, respectively. **(D)** Nine different anti-α-Syn antibodies (epitopes in Table S1) detect inclusions in *SNCA*$^{-/-}$ neurons transfected with hα-Syn. **(E)** hα-Syn inclusions in transfected *SNCA*$^{-/-}$ neurons exhibit LB-like pathology, as they are positive to Thioflavin-S (lower panel), are phosphorylated at S129 (upper panel) and are ubiquitinated (middle panel). Co-localization was confirmed by assessing regression coefficients (R^2) of signals of both channels (shown in the upper right corner of the merged images). Scale bars denote 10 µm in "A-B" and 5 µm in "D-E".

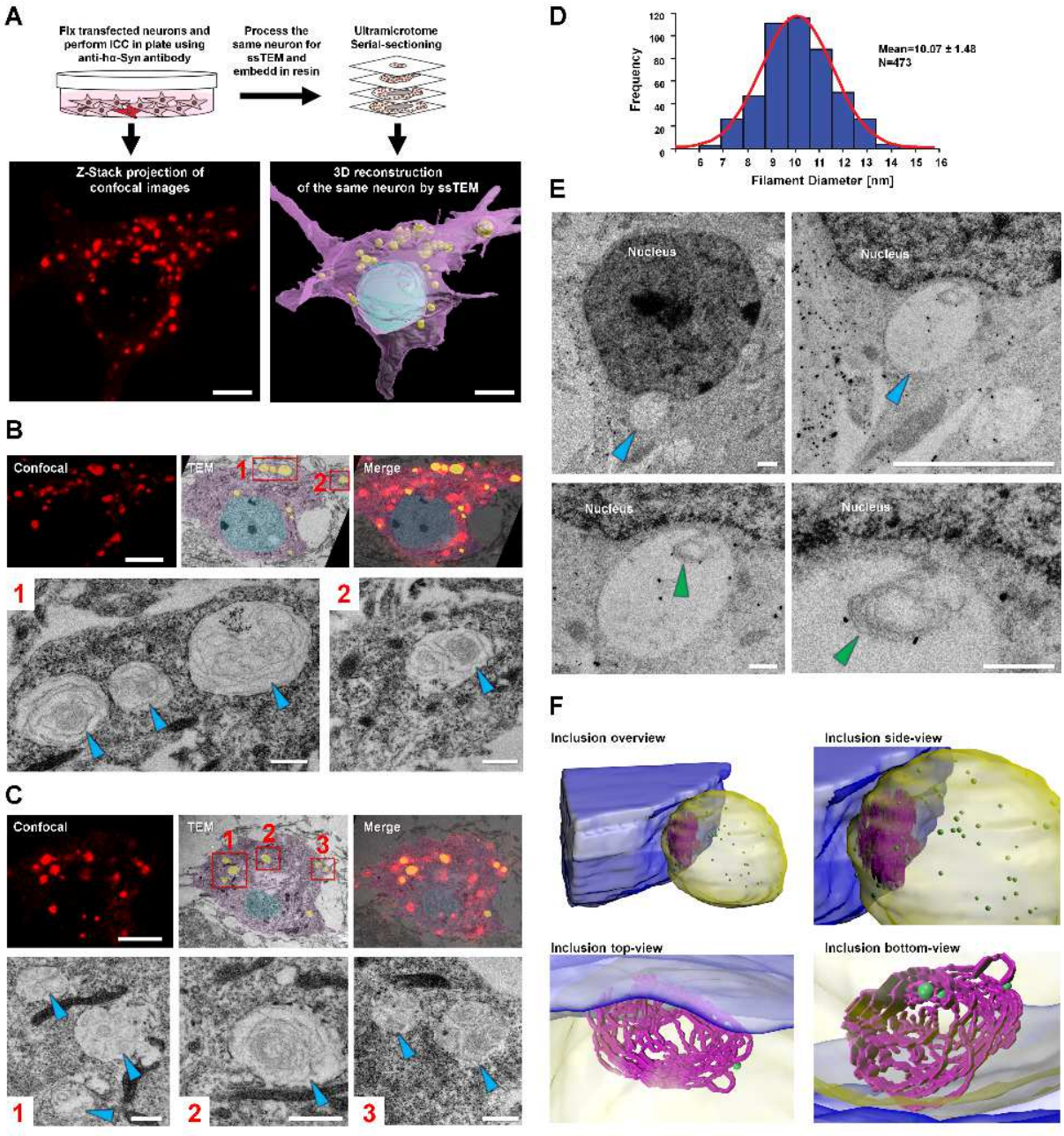

Fig. 2. Ultrastructure of hα-Syn inclusions in *SNCA*$^{-/-}$ neurons. **(A)** For CLEM analysis, a stained neuron was imaged by confocal microscopy, and then reprocessed and imaged by TEM resulting in a high resolution 3D acquisition of the same neuron. For illustration, the nucleus is rendered in blue, the cytosol in purple and inclusions in yellow. Scale bars denote 5µm. **(B)** To correlate between structures observed by ssTEM and fluorescence, single plane images were super-imposed (upper panel). High resolution images of inclusions (red boxes 1 and 2) are shown in the lower panel, with arrows indicating filamentous structures. The scale bar denotes 5 and 2 µm in the upper and lower panel, respectively. **(C)** The same analysis as in (B) but on different confocal and ssTEM planes from the same neuron shows heterogeneous filamentous content. **(D)** Most filaments observed by ssTEM (n=473) have a width ranging from 7-13 nm. The normal curve is shown in red, as well as values of mean ± SD. **(E)** Immuno-gold labelling of *SNCA*$^{-/-}$

neurons expressing hα-Syn with the ab-6176 anti-Synuclein antibody establishes that filaments are positive for Synuclein. Four ssTEM images of different magnifications of the inclusion (blue arrowhead) and filaments (green arrowhead) are shown. The scale bar denotes 1 µm in the upper panel and 125 nm in the lower panel. **(F)** A 3D model of the inclusion (blue arrow in "E") reveals a mesh of intertwining filamentous structures (in purple) with gold particles reacting with inner and outer portions. For illustration, the nucleus is rendered in blue, the inclusion in yellow, and immuno-gold particles in green.

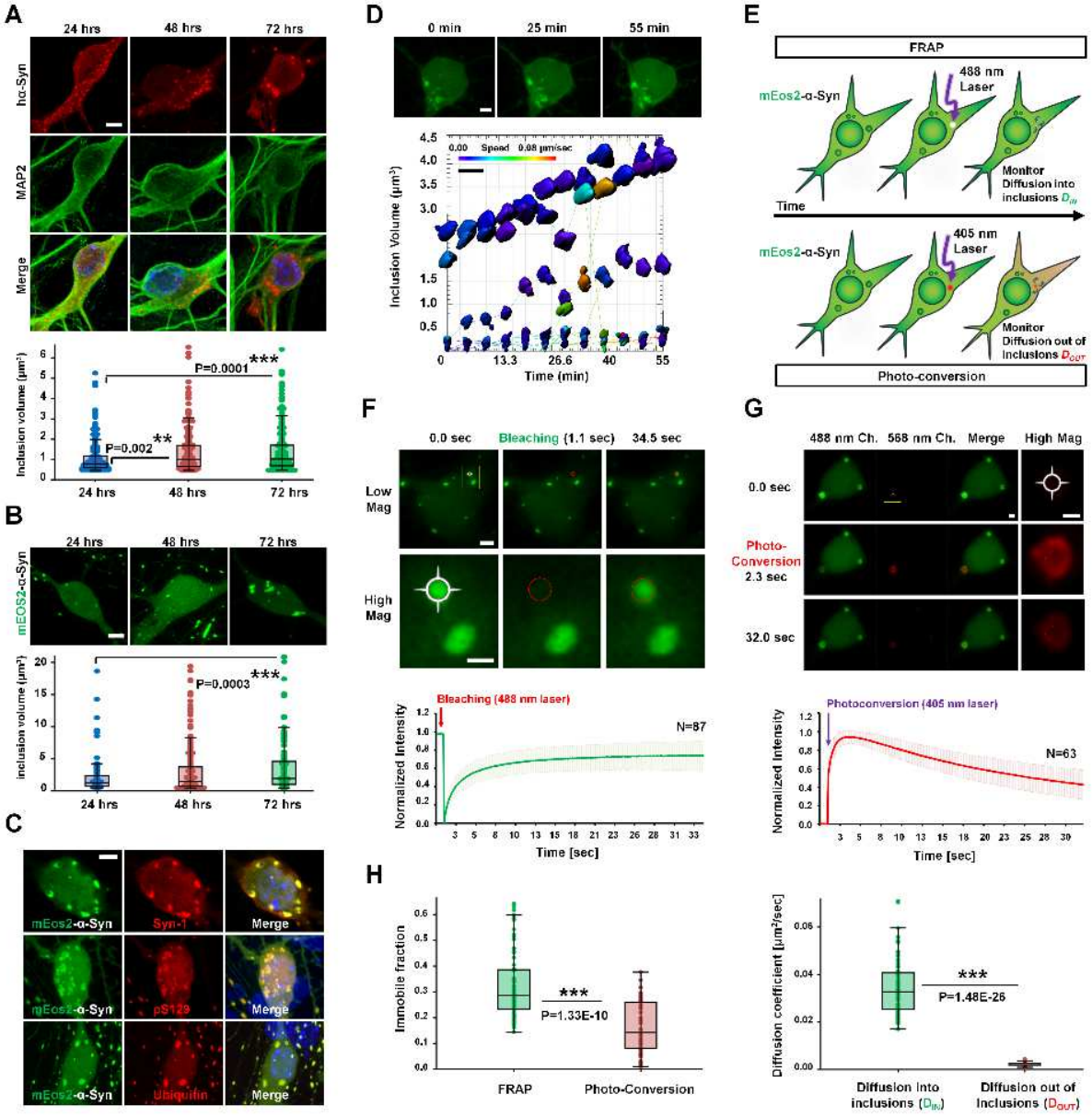

Fig. 3. hα-Syn inclusions in *SNCA*$^{-/-}$ neurons grow and incorporate soluble hα-Syn. (A) hα-Syn inclusions form 24 hrs post-transfection and grow over the next 24 hrs. 3D inclusion rendering and

quantification (n=25 neurons per condition) reveals significant inclusion volume increase at 48 and 72 hrs in MAP2 positive neurons. (**B)** mEOS2-α-Syn inclusions form 24 hrs post-transfection and grow over 72 hrs of live imaging. 3D inclusion rendering and quantification (50 neurons per condition) reveals significant inclusion volume increase 72 hrs post-transfection. **(C)** mEOS2-α-Syn inclusions are immuno-positive for total α-Syn (Syn-1), pS129-α-Syn (WAKO) and ubiquitin. **(D)** mEOS2-Syn inclusions are immobile, and individually grow over ~1 hr of live imaging. Scale bars denote 5 µm in "A-C", and 2 µm in "D". **(E)** In FRAP experiments, inclusions were photo-bleached, and fluorescence recovery from diffusing soluble protein was monitored. In photo-conversion experiments, inclusion fluorescence was photo-converted from 488 nm to 568 nm, and 568 nm fluorescence decay by diffusion out of inclusions was monitored. Fluorescence before, during and after inclusion (crossed circles) photo-bleaching **(F)** or photo-conversion **(G)** is shown. Middle panels show higher magnification of yellow boxes. Bottom panels show average plots (± SD) of normalized FRAP or photo-conversion (568 nm channel) recovery curves (n=87 or 63 inclusions, respectively). Scale bars denote 2 and 1 µm in lower and higher magnifications. **(H)** Values for immobile fractions and diffusion coefficients obtained from photo-conversion curves (n=50 inclusions) are significantly lower than those obtained by FRAP. In "A-B and H", the Mann-Whiney test was applied to obtain P values (overlayed on box plots/violin scatter plots of individual values).

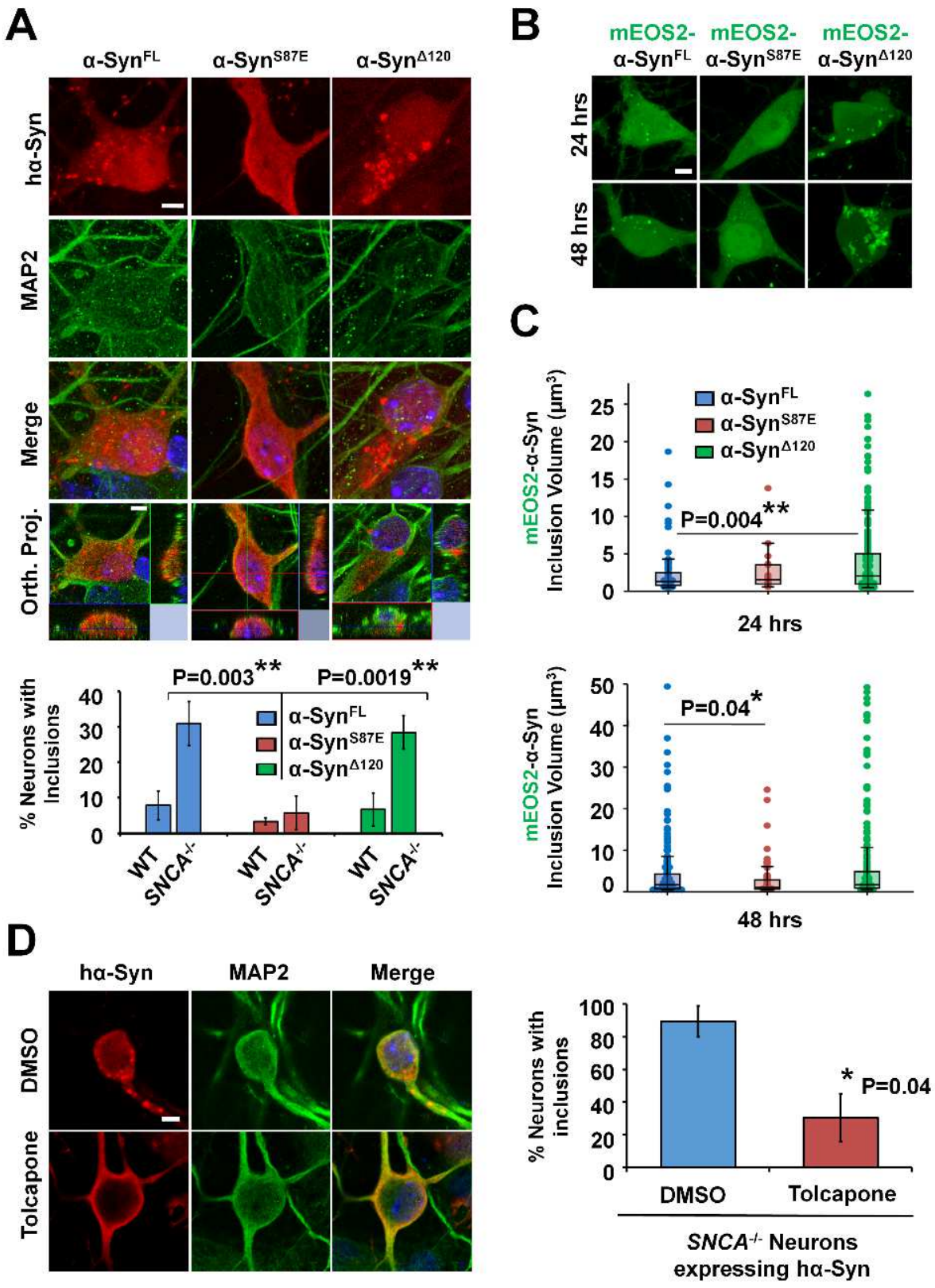
A
α-Syn^FL
α-Syn^S87E
α-Syn^Δ120
hα-Syn
MAP2
Merge
Orth. Proj.
% Neurons with Inclusions
P=0.003**
P=0.0019**
α-Syn^FL
α-Syn^S87E
α-Syn^Δ120
WT
SNCA-/-
B
mEOS2-α-Syn^FL
mEOS2-α-Syn^S87E
mEOS2-α-Syn^Δ120
24 hrs
48 hrs
C
mEOS2-α-Syn Inclusion Volume (μm³)
P=0.004**
24 hrs
P=0.04*
48 hrs
D
hα-Syn
MAP2
Merge
DMSO
Tolcapone
% Neurons with inclusions
* P=0.04
DMSO
Tolcapone
SNCA-/- Neurons expressing hα-Syn

Fig. 4. Inclusion formation in *SNCA*$^{-/-}$ neurons reflects a hα-Syn aggregation driven process. (A) Whereas both hα-Syn^{FL} and hα-Syn$^{\Delta 120}$ form inclusions, the S87E aggregation deficient variant exhibits diffuse localization in *SNCA*$^{-/-}$ neurons 48 hrs post-transfection. Quantification of inclusion formation (>1µm) in 25 neurons per condition (mean ± SD, n=3 independent experiments) shows that significantly less α-Syn^{S87E} expressing neurons develop inclusions compared to α-Syn^{FL} and Syn$^{\Delta 120}$ counterparts. **(B)** Live imaging of *SNCA*$^{-/-}$ neurons expressing mEOS2-α-Syn^{FL}, mEOS2-α-Syn^{S87E} or mEOS2-α-Syn$^{\Delta 120}$ 24 hrs or 48 hrs post-transfection shows that mEOS2-α-Syn^{S87E} does not form prominent inclusions at both time-points. **(C)** 3D rendering of inclusion volume over 48 hrs post-transfection (50 neurons per condition) shows that whereas mEOS2-α-Syn$^{\Delta 120}$ forms significantly larger inclusions 24 hrs post-transfection compared to mEOS2-α-Syn^{WT}, the mEOS2-α-Syn^{S87E} mutant forms smaller inclusions at 48 hrs. Box plots overlaying violin scatter plots of individual values are shown. **(D)** *SNCA*$^{-/-}$ neurons expressing hα-Syn for 24 hrs were treated either with DMSO or 20µM Tolcapone for an additional 24 hrs. Whereas DMSO treated neurons develop inclusions, those treated with Tolcapone exhibit diffuse hα-Syn localization. Quantification of inclusion formation (>1µm) in 25 neurons per condition (mean ± SD, n=3 independent experiments) shows that significantly less tolcapone treated transfected neurons develop inclusions compared to DMSO treated controls (right panel). In all panels scale bars denote 5 µm. In "A" one-way ANOVA/Scheff*é* test was applied, whereas in "C-D" the Mann-Whiney test was applied to obtain P values (overlayed on plots).

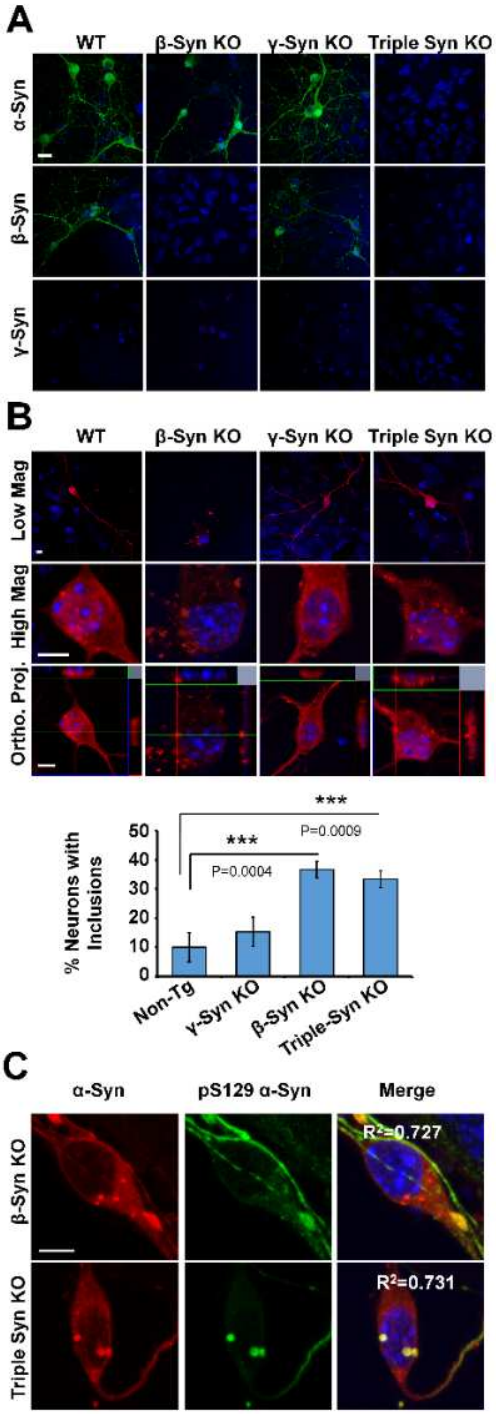

Fig. 5. Endogenous β-Syn KO naturally also acts as a hα-Syn aggregation inhibitor in primary neurons. (A) Immuno-cytochemistry validates loss of α- and β-Syn expression in α-Syn KO, β-Syn KO and triple Syn KO neurons compared to WT neurons. In contrast, γ-Syn immunoreactivity was not detected across conditions. **(B)** hα-Syn exhibits diffuse distribution in WT and γ-Syn KO transfected neurons, and forms inclusions (>1 µm) in cell bodies and neurites of β-Syn KO and triple Syn KO neurons. Quantification of 20 neurons per condition (mean ± SD, n=3 independent experiments) shows that significantly more β-

Syn KO neurons and Triple KO neurons (one-way ANOVA, Scheffé) develop inclusions (>1 µm in diameter) compared to non-Tg neurons. **(C)** Inclusions formed in β-Syn KO and triple Syn KO neurons are hyper-phosphorylated at S129. Co-localization was confirmed by assessing regression coefficients (R^2) of signals of both channels. The scale bar denotes 20 µm in "A", and 5 µm in B-C.

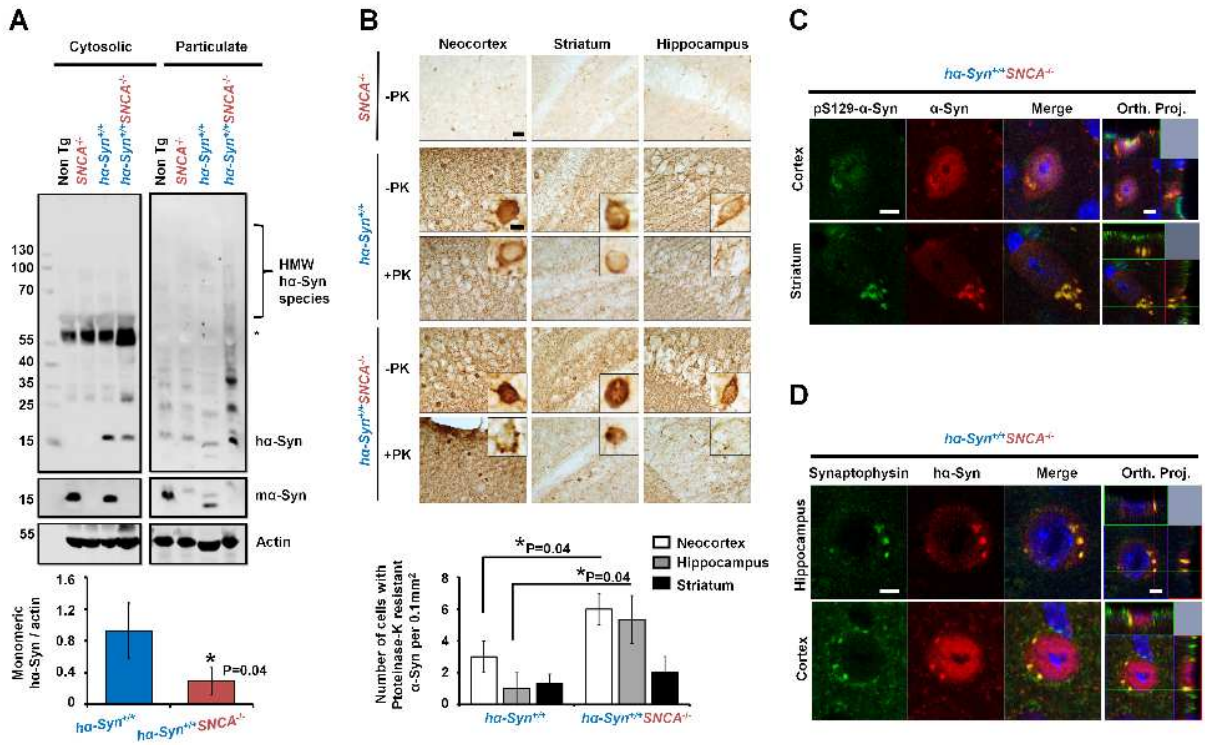

Fig. 6. The absence of mα-Syn promotes hα-Syn aggregation transgenic mice. (A) Less monomeric hα-Syn is detected in detergent-soluble fractions from *hα-Syn*$^{+/+}$*SNCA*$^{-/-}$ mice compared to *hα-Syn*$^{+/+}$ counterparts, concomitant with appearance of HMW hα-Syn species in detergent-insoluble fractions. Loss of mα-Syn expression in *SNCA*$^{-/-}$ mice is verified using the mα-Syn specific antibody D37A6, and actin denotes equal protein loading. The asterisk refers to a nonspecific band. Densitometric quantification (n=3 independent experiments) shows significantly decreased levels of cytosolic hα-Syn when expressed on *SNCA*$^{-/-}$ background. **(B)** *hα-Syn*$^{+/+}$ and *hα-Syn*$^{+/+}$*SNCA*$^{-/-}$ mice brains show strong hα-Syn expression in the neocortex, striatum and hippocampus that weakens upon PK treatment. High magnification analysis (insets) reveals intense proteinase-K resistant hα-Syn inclusions in *hα-Syn*$^{+/+}$*SNCA*$^{-/-}$ mice. Scale bars denote 100 µm in overviews and 15 µm in insets. Quantification of the number of cells with proteinase-K resistant hα-Syn inclusions per 0.1 mm^2 (n= 3 mice per condition) shows that significantly more inclusion bearing cells are detected in the neocortex and hippocampus of *hα-Syn*$^{+/+}$*SNCA*$^{-/-}$ mice compared to *hα-Syn*$^{+/+}$ *mice*. In "A-B", the Mann-Whiney test was applied to obtain P values (overlayed on histograms showing mean ± SD). **(C-D)** Double positive hα-Syn inclusions for total α-Syn and pS129 α-Syn (C) or synaptophysin (D)

are detected in the cortex, striatum and hippocampus of *hα-Syn*$^{+/+}$*SNCA*$^{-/-}$ mice. Orthogonal Z-stacks projections verify intracellular nature of inclusions. Scale bar denotes 5 µm.

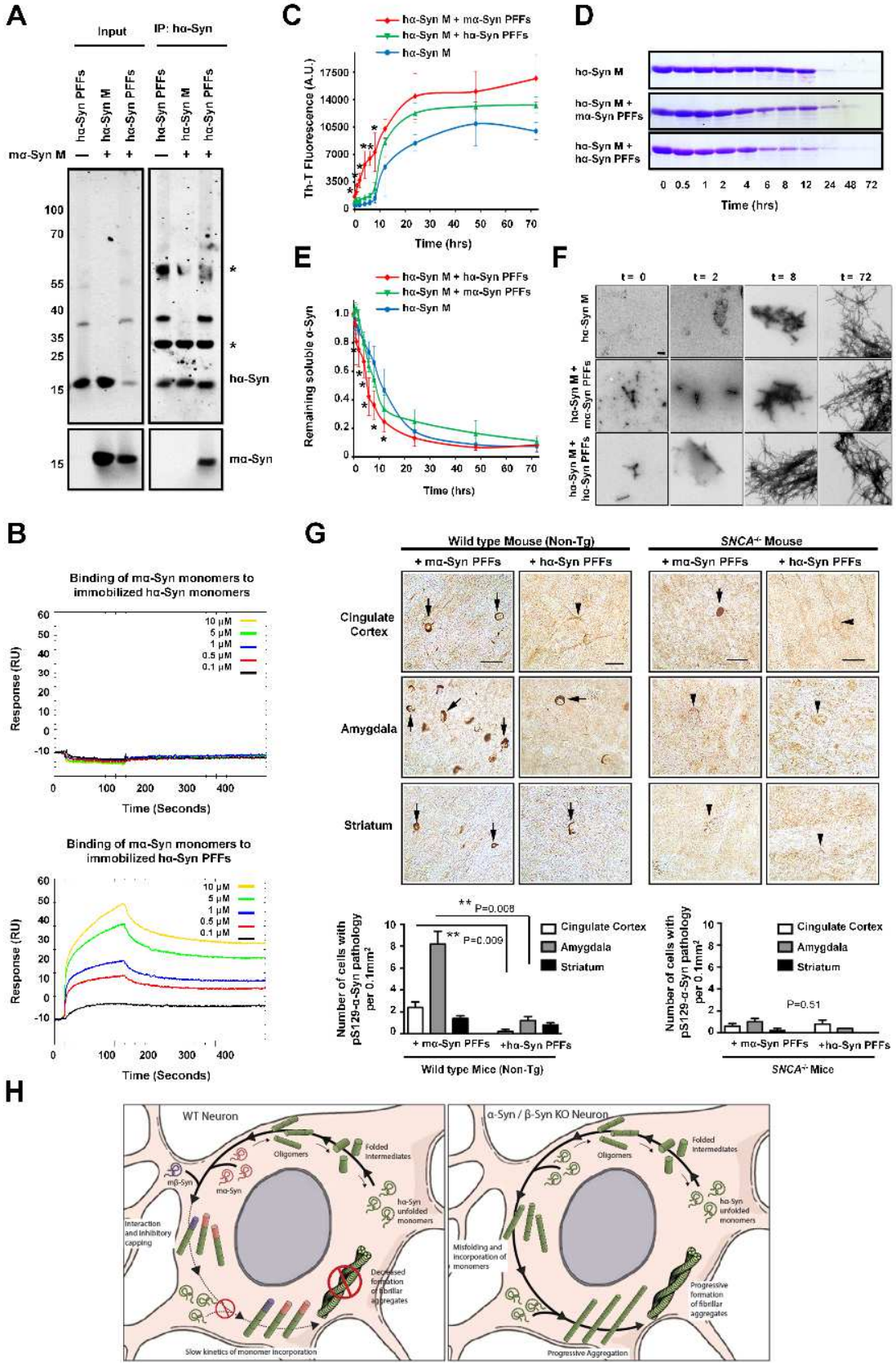
A
Input
IP: hα-Syn
hα-Syn PFFs
hα-Syn M
hα-Syn PFFs
hα-Syn PFFs
hα-Syn M
hα-Syn PFFs
mα-Syn M — + + — + +
100
70
55
40
35
25
15
15
*
*
hα-Syn
mα-Syn
B
Binding of mα-Syn monomers to immobilized hα-Syn monomers
Response (RU)
Time (Seconds)
10 µM
5 µM
1 µM
0.5 µM
0.1 µM
Binding of mα-Syn monomers to immobilized hα-Syn PFFs
Response (RU)
Time (Seconds)
10 µM
5 µM
1 µM
0.5 µM
0.1 µM
C
hα-Syn M + mα-Syn PFFs
hα-Syn M + hα-Syn PFFs
hα-Syn M
Th-T Fluorescence (A.U.)
Time (hrs)
D
hα-Syn M
hα-Syn M + mα-Syn PFFs
hα-Syn M + hα-Syn PFFs
0 0.5 1 2 4 6 8 12 24 48 72
Time (hrs)
E
hα-Syn M + hα-Syn PFFs
hα-Syn M + mα-Syn PFFs
hα-Syn M
Remaining soluble α-Syn
Time (hrs)
F
t = 0
t = 2
t = 8
t = 72
hα-Syn M
hα-Syn M + mα-Syn PFFs
hα-Syn M + hα-Syn PFFs
G
Wild type Mouse (Non-Tg)
SNCA-/- Mouse
+ mα-Syn PFFs
+ hα-Syn PFFs
+ mα-Syn PFFs
+ hα-Syn PFFs
Cingulate Cortex
Amygdala
Striatum
** P=0.008
** P=0.009
Number of cells with pS129-α-Syn pathology per 0.1mm²
Cingulate Cortex
Amygdala
Striatum
+ mα-Syn PFFs
+hα-Syn PFFs
Wild type Mice (Non-Tg)
P=0.51
Number of cells with pS129-α-Syn pathology per 0.1mm²
Cingulate Cortex
Amygdala
Striatum
+ mα-Syn PFFs
+hα-Syn PFFs
SNCA-/- Mice
H
WT Neuron
α-Syn / β-Syn KO Neuron
Oligomers
Folded Intermediates
mβ-Syn
mα-Syn
hα-Syn unfolded monomers
Interaction and inhibitory capping
Decreased formation of fibrillar aggregates
Slow kinetics of monomer incorporation
Misfolding and incorporation of monomers
Progressive formation of fibrillar aggregates
Progressive Aggregation

Fig. 7. mα-Syn interacts with aggregated hα-Syn species and attenuates seeding and spreading. (A) mα-Syn monomers (M) were incubated with equimolar amounts of hα-Syn M or sonicated fibrils (PFFs) before immuno-precipitation (IP) of hα-Syn. Following IP, mα-Syn was detected only in the sample comprising the mixture of mα-Syn and hα-Syn PFFs. Input solutions show similar protein levels before IP. The asterisks denote the heavy and light chains of the antibody used for IP. **(B)** hα-Syn M or hα-Syn PFFs were immobilized on a CM5 chip, and then increasing concentrations of mα-Syn M were flushed in to assess interaction kinetics by surface plasmon resonance (SPR). A response (interaction) was noted between immobilized hα-Syn PFF and injected mα-Syn M, and not with hα-Syn M. **(C-F)** hα-Syn M were incubated either alone (20 μM) or with 10% sonicated hα-Syn PFFs or mα-Syn PFFs, and aggregation kinetics were followed by: **(C)** ThT fluorescence, **(D-E)** assessing remaining soluble protein and **(F)** TEM analysis. **(C-E)** Quantification of 3 independent experiments shows that mixtures of hα-Syn PFFs + hα-Syn M exhibit significantly higher ThT binding **(C)** and less soluble protein content **(D-E)** compared to hα-Syn M + mα-Syn PFFs at early time-points (0-12 hours). The Mann-Whiney test was applied to obtain P values (P=0.04) from, and values of mean ± SD are shown. **(F)** TEM analysis shows that mixtures of hα-Syn PFFs + hα-Syn M start forming fibrils after 8 hrs, compared to hα-Syn M alone or with mα-Syn PFFs which form oligomeric species at this timepoint. After 72 hrs, all three conditions show fibrillar morphology. **(G)** Immunohistochemistry shows compact somatic pS129-α-Syn inclusions (arrows) in the cingulate cortex, amygdala and striatum of WT mice injected with mα-Syn PFFs. In contrast, injection of hα-Syn PFFs in WT mice resulted in diffuse staining (arrowheads) in the cingulate cortex, and few somatic inclusions in the amygdala and striatum. Likewise, injection of either hα-Syn PFFs or mα-Syn PFFs in *SNCA*$^{-/-}$ mice resulted mostly in diffuse localization, with very few detected inclusions. Quantification of the number of cells showing pS129-α-Syn pathology per 0.1 mm^2 (n= 5 mice per condition; mean ± SD) shows significantly more inclusions (Mann-Whitney test) in the cingulate cortex and amygdala of WT mice injected with mα-Syn PFFs compared to hα-Syn PFFs. In in *SNCA*$^{-/-}$ mice, no differences were noted across conditions. The scale bar denotes 200 nm in F and 100 μm in G. **(H)** Potential mechanism of hα-Syn aggregation inhibition by endogenous mα-Syn or mβ-Syn. In WT neurons, over-expressed monomeric hα-Syn (green) misfolds into aggregation prone intermediates that form oligomers/protofibrils. Endogenous mα-Syn monomers (in red) or mβ-Syn (purple) preferentially interact with these hα-Syn species. This interaction attenuates the progressive incorporation of hα-Syn monomers, resulting in slower aggregation kinetics and decreased fibril formation. In *SNCA*$^{-/-}$ neurons or β-Syn KO neurons, as the combined levels of endogenous mα-Syn and mβ-Syn falls below a certain threshold, the inhibitory capping mechanism is reduced, and thus over-expressed hα-Syn aggregates more readily.